in a cell cycle–dependent manner. Only four of these (DivJ, CckA, PleC, and CheA) have been characterized, and three of the four (boxed in Fig. 4) are known to be dynamically localized to the cell poles at different times in the cell cycle (*21, 22*). The spatial distribution of CtrA also varies during the cell cycle (Fig. 1A) (*20*); together, these observations add another regulatory dimension. The operation of *Caulobacter*'s genetic circuitry controlling cell cycle progression and asymmetric cell division must ultimately be analyzed and modeled as an integrated, three-dimensional system of coupled chemical reactions incorporating genome-scale information on mRNA and protein levels, posttranslation modifications, and spatial distributions.

References and Notes

1. D. Hung, H. McAdams, L. Shapiro, in *Prokaryotic Development*, Y. V. Brun, L. J. Shimkets, Eds. (ASM Press, Washington, DC, 2000), pp. 361–378.
2. For complete data sets, gene lists, and details of microarray procedures, see http://caulobacter.stanford.edu/CellCycle.
3. P. T. Spellman *et al.*, *Mol. Biol. Cell* **9**, 3273 (1998).
4. R. J. Cho *et al.*, *Mol. Cell* **2**, 65 (1998).
5. For complete methods (including experimental procedures, details of the discrete cosine transform algorithm, clustering analyses, and promoter analysis), as well as annotated figures and a listing of all previously characterized genes (with references), see *Science* Online (www.sciencemag.org/cgi/content/full/290/5499/2144/DC1).
6. M. T. Laub, H. H. McAdams, T. Feldblyum, L. Shapiro, data not shown.
7. A complete functional categorization of the 553 cell cycle–regulated genes is available (5).
8. D. A. Mohl, J. W. Gober, *Cell* **88**, 675 (1997).
9. G. C. Draper, H. H. Ho, J. W. Gober, *Interactions Between GidA and the Chromosome Partitioning Apparatus of* Caulobacter crescentus (published in abstracts of the American Society for Microbiology General Meeting, Los Angeles, June 2000).
10. E. A. O'Neill, R. A. Bender, *J. Bacteriol.* **169**, 2618 (1987).
11. H. Iba, A. Fukuda, Y. Okada, *J. Bacteriol.* **135**, 647 (1978).
12. A. Newton, *Proc. Natl. Acad. Sci. U.S.A.* **69**, 447 (1972).
13. J. W. Gober, J. C. England, in *Prokaryotic Development*, Y. V. Brun, L. J. Shimkets, Eds. (ASM Press, Washington, DC, 2000), pp. 319–339.
14. J. M. Skerker, L. Shapiro, *EMBO J.* **19**, 3223 (2000).
15. N. Ohta, T. W. Grebe, A. Newton, in *Prokaryotic Development*, Y. V. Brun, L. J. Shimkets, Eds. (ASM Press, Washington, DC, 2000), pp. 341–359.
16. K. C. Quon, G. T. Marczynski, L. Shapiro, *Cell* **84**, 83 (1996).
17. K. C. Quon, B. Yang, I. J. Domian, L. Shapiro, G. T. Marczynski, *Proc. Natl. Acad. Sci. U.S.A.* **95**, 120 (1998).
18. D. Missiakas, S. Raina, *Mol. Microbiol.* **28**, 1059 (1998).
19. M. T. Laub, unpublished data.
20. I. J. Domian, K. C. Quon, L. Shapiro, *Cell* **90**, 415 (1997).
21. R. T. Wheeler, L. Shapiro, *Mol. Cell* **4**, 683 (1999).
22. C. Jacobs, I. J. Domian, J. R. Maddock, L. Shapiro, *Cell* **97**, 111 (1999).
23. I. J. Domian, A. Reisenauer, L. Shapiro, *Proc. Natl. Acad. Sci. U.S.A.* **96**, 6648 (1999).

24. *Caulobacter* sequence data were provided by The Institute for Genomic Research (W. O. Nierman *et al.*, submitted). Sequencing of *C. crescentus* was accomplished with support from the U.S. Department of Energy. We thank K. Keiler and K. Ryan for helpful discussions, K. Ryan for strains LS3326 and LS3327, and J. Wang and S. Kim for assistance in microarray manufacturing. Supported by a Howard Hughes Medical Institute predoctoral fellowship and a Stanford Graduate Fellowship (M.T.L.), NIH grants GM32506 and GM51426 (L.S.), and Defense Advanced Research Projects Agency–Office of Naval Research grant N00014-99-1-05631 (H.H.M.).

17 August 2000; accepted 16 October 2000

The Bacterial Flagellar Cap as the Rotary Promoter of Flagellin Self-Assembly

Koji Yonekura,[1]* Saori Maki,[1]* David Gene Morgan,[2] David J. DeRosier,[3] Ferenc Vonderviszt,[4] Katsumi Imada,[1] Keiichi Namba[1,5]†

The growth of the bacterial flagellar filament occurs at its distal end by self-assembly of flagellin transported from the cytoplasm through the narrow central channel. The cap at the growing end is essential for its growth, remaining stably attached while permitting the flagellin insertion. In order to understand the assembly mechanism, we used electron microscopy to study the structures of the cap-filament complex and isolated cap dimer. Five leg-like anchor domains of the pentameric cap flexibly adjusted their conformations to keep just one flagellin binding site open, indicating a cap rotation mechanism to promote the flagellin self-assembly. This represents one of the most dynamic movements in protein structures.

Self-assembly is used in biological systems to construct large molecular complexes and cellular organelles. In most cases, the assembly processes are regulated by conformational adaptability between the assembled proteins and those that form the site of assembly. The assembly mechanism is not based on simple lock-and-key interactions of compactly folded molecules but involves dynamic conformational changes and partial folding. Tobacco mosaic virus (*1*, *2*) and the bacterial flagellum (*3*, *4*) are classical examples of such mechanisms. These two systems vividly illustrate how the conformational flexibility and adaptability of biological macromolecules regulate the assembly processes. However, the structures of the assembly sites have never been visualized, even for these well-defined structures. In order to study the assembly process of the bacterial flagellar filament, we have used electron microscopy and single particle image analysis.

In many bacteria, swimming results from rotation of helical flagella driven by rotary motors at their bases (*5–7*). In *Escherichia coli* and *Salmonella*, the motor structure called the flagellar basal body crosses both cytoplasmic and outer membrane and continues as an extracellular structure called the hook and the filament. The assembly process starts with FliF ring formation in the cytoplasmic membrane (*8*) (Fig. 1A). A dedicated export apparatus, homologous to the type III protein export system (*9*), is believed to be integrated at the cytoplasmic opening of the FliF ring channel and to export selectively a set of flagellar proteins into the channel in the flagellum by using the energy of ATP hydrolysis (*10*, *11*). The flagellar proteins travel through the channel of the growing structure to the distal end, where the assembly occurs (*12*, *13*). The filament is only about 200 Å in diameter but grows to a length of up to 15 μm by polymerization of as many as 30,000 flagellin subunits. The central channel through which those flagellin subunits are transported is only 30 Å wide. The entire flagellum is built by self-assembly of the component proteins.

Just before the filament elongation starts in the growth process of the bacterial flagellum, HAP2 (hook-associated protein 2, also called FliD) forms a cap on top of the hook-HAP1-HAP3 complex (*14*). Then, flagellin subunits passing through the channel polymerize just below the cap one after another to form the long helical filament (*15*) (Fig. 1A). The cap stays attached at the distal end during the filament growth, and the simplest role of

[1]Protonic NanoMachine Project, ERATO, JST, 3-4 Hikaridai, Seika, Kyoto 619-0237, Japan. [2]Department of Biophysics, Boston University School of Medicine, Boston, MA 02118, and Department of Cell Biology, Harvard Medical School, Boston, MA 02254, USA. [3]Rosenstiel Basic Medical Sciences Research Center, Brandeis University, Waltham, MA 02254, USA. [4]Department of Physics, University of Veszprém, Egyetem Street 10, H-8201 Veszprém, Hungary. [5]Advanced Technology Research Laboratories, Matsushita Electric Industrial Co., Ltd., 3-4 Hikaridai, Seika, Kyoto 619-0237 Japan.

*These authors contributed equally to this work.
†To whom correspondence should be addressed. E-mail: keiichi@crl.mei.co.jp

the cap would be to prevent flagellin from leaking out (*15–17*). However, HAP proteins are occasionally transported and pass through the capped end (*18*). The cap may also induce a conformational change in flagellin for polymerization. For insertion of flagellin subunits, the cap must move up by steps to make room for the next flagellin monomer. Thus the cap must play apparently contradictory roles: It must remain stably attached while permitting the insertion of flagellin subunits.

We have analyzed the structure of the reconstituted cap-filament complex by electron cryomicroscopy of a frozen hydrated sample in order to visualize how the cap functions to perform the contradictory roles described above. It was a challenge to visualize such a small structure at the end of the long periodic structure, but we managed to develop a method to perform the task (*19*). A few typical examples of raw images are presented, which show the low contrast and high level of noise typical of cryomicrographs (Fig. 1B). We collected many of those images for three-dimensional image reconstruction by back projection. After two-dimensional alignment and averaging of many of these images, the resultant averaged image (Fig. 1C) clearly showed the density distributions of distinct domains. The inner and outer tubes extended over radial ranges from 15 to 30 Å (domain D0) and from 35 to 60 Å (D1), respectively, in the core of the filament, the outer domains of flagellin from 60 to 115 Å in radius (D2 and D3), and a thin, plate-like cap with a large cavity underneath.

In the reconstructed three-dimensional density map, the filament portion showed the expected helical array of the outer domains of flagellin subunits (Fig. 2),[7] as in the previous maps produced by helical image reconstruction (*20*, *21*). The array of these outer domains could be traced along the 1-start helix of the filament, a very shallow, right-handed helix with a pitch of about 26 Å containing approximately 11 subunits per two turns. Because the chain of subunits was unbroken along the 1-start helix, the assembly of subunits is likely to proceed along the 1-start helix.

The lid-like plate or cap at the top was 120 Å wide and 25 Å thick; the diameter was roughly the same as that of the outer tube of the filament (domain D1). Its pentagonal shape in the end-on view (Fig. 2A) indicated that the cap is a pentamer of HAP2, half of the decamer complex formed in solution (*22*, *23*). This pentagonal plate is attached to the distal end of the filament at five positions through its anchor domains, where these anchor domains show significant deviation from the five-fold symmetry. The five anchor domains are well separated from one another, forming five gaps with different sizes and shapes between the plate and the filament end (Fig. 2C). One of the gaps (Fig. 2C-1) is distinctly larger than the other four, having an inverted L shape. The wide portion of this gap has a vertical dimension of about 50 Å with a width of 25 Å, which corresponds to the size of domain D1 of flagellin (*24*, *25*). Domain D1 is axially elongated and composed of axially aligned α helices (*26*). Because of the axial stagger in the lateral subunit packing, the end of the filament is not flat but has five indentations around its circumference, one of which is a double indentation. With the HAP2 plate in place, these indentations in the filament end become openings of different sizes from the central channel to the exterior of the filament (discussed below). The opening having an inverted L shape has the characteristic shape and size of the double indentation, and this is the only one large enough to accommodate domain D1. Thus, this is most likely to be the site of flagellin assembly.

Inside the filament just below the cap plate, there is a cavity roughly 40 Å wide and 70 Å deep (Fig. 2, D and E). In the filament's interior, the cavity widens up to 60 Å for about 15 Å and suddenly narrows down to the central channel of the filament, about 30 Å wide. Because 30 Å and 60 Å are the inner diameters of the inner and outer tubes, respectively, the narrower part of the cavity just below the plate is likely to be narrowed by the anchor domains of HAP2 extending into the cavity at a slightly smaller radius than that of the outer tube. However, because of the limited resolution of the map, individual anchor domains cannot be distinguished from the outer-tube domains of flagellin.

Each domain of flagellin may be thin enough to be accommodated in the channel, but because the folded flagellin molecule has a kink in the middle, it cannot pass through the channel (*20*, *21*, *26*). Flagellin would need to be unfolded or at least have its domains drastically rearranged before it reaches the distal end. This cavity may play some role in helping flagellin to fold up, perhaps in a way similar to Anfinsen's cage in chaperonin (*27*). The cavity appears to have the right size to accommodate only one flagellin subunit, allowing its refolding without aggregation with other subunits.

The HAP2 protein forms a decameric complex in solution (*22*). The decamer observed by electron microscopy shows a pentameric feature in its end-on view (*28*) and a bipolar structure with two thin plates connected by a pair of long, slightly tapered cylindrical walls in its side view (*23*). The connecting portion appeared to be relatively flexible. We carried out a single particle analysis to deduce the three-dimensional structure (*29*) (Fig. 3). The structure showed a bipolar pair of the pentamers; each pentamer was composed of a pentagonal plate and five leg domains. The two pentamers were connected with a domain with no particular feature at the center. This portion is made of both terminal regions, because when about 40 NH_2-terminal and 50 COOH-terminal residues of HAP2, which are disordered in the pentameric or

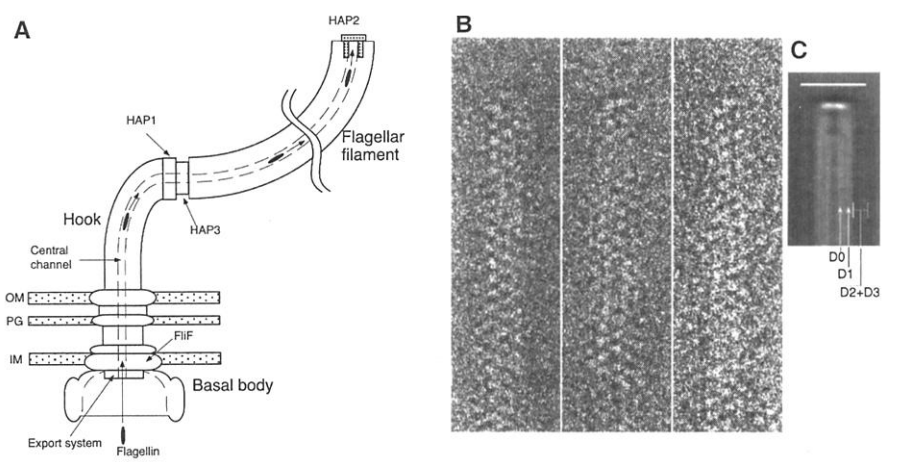

Fig. 1. Schematic diagram describing the assembly process of the bacterial flagellar filament and electron cryomicrographs of the frozen hydrated cap-filament complex. (**A**) Filament growth by polymerization of flagellin below the cap. Flagellin is exported though the central channel to the distal end of the flagellum. OM, outer membrane; PG, peptidoglycan layer; IM, cytoplasmic membrane. (**B**) Electron cryomicrographs of the cap-filament complex. The thin, flat plate at the top of the filament is barely seen. (**C**) Average composite of 589 images of the cap-filament complex after two-dimensional alignment. The cap is clearly visible as well as the domains of flagellin in the filament portion, which are labeled D0 (the inner tube), D1 (the outer tube), and D2+D3 (the outer domains). The density of the filament portion is axially continuous because the image is equivalent to the result of cylindrical averaging. The weak density of the outer domains is caused by the cylindrical average of well-separated domains. Scale bar, filament diameter of 230 Å.

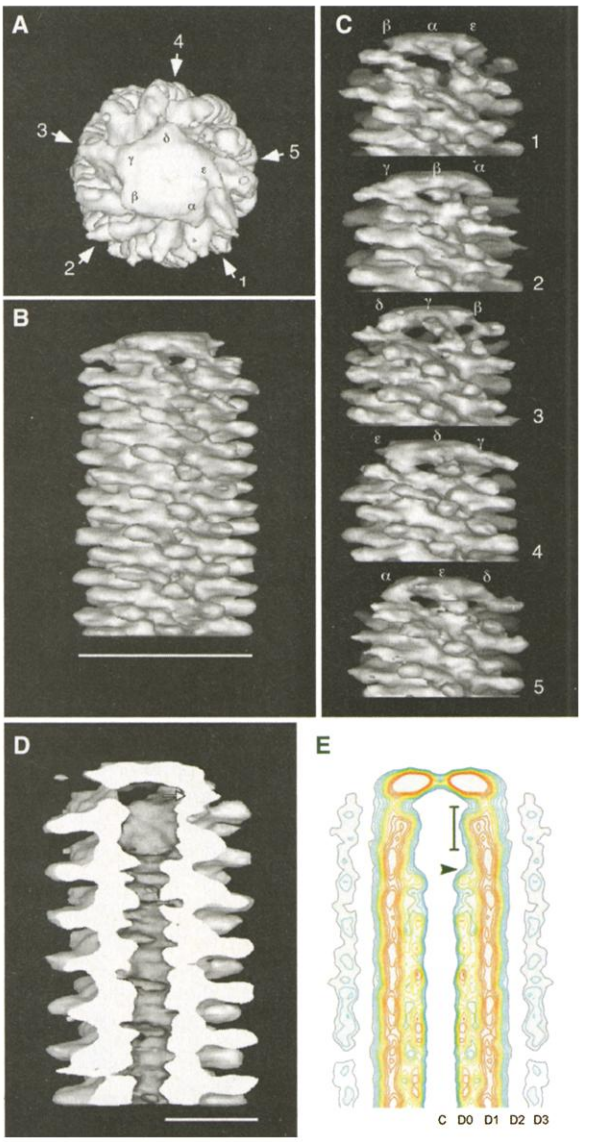

Fig. 2. Three-dimensional density map of the cap-filament complex and its central section. (**A**) End-on view from the top, showing a pentagonal shape of the plate domain of the cap. The five vertices of the pentagon are labeled with Greek letters, α to ε, which are used to guide the orientation of the pentagon in the side views in (C). (**B**) Side view, showing a regular helical array of flagellin subunits and the plate domain of the cap. Scale bar, filament diameter of 230 Å. (**C**) Five side views, showing each of the five gaps between the plate and the filament end. The viewing directions are as indicated by arrows in (A) labeled with corresponding numbers. Greek letters labeling the vertices as in (A) also indicate the orientations of the pentagonal plate. Note that part of the gap in view 1 has an axial extension that is significantly larger than that of the other four gaps and this is likely to be the site of assembly for the newly arriving flagellin subunit. (**D**) Structure of the cap-filament complex cut out at the plane containing the filament axis and viewed from the side. The cavity below the plate and the central channel of the filament are shown. The density below the plate on the right side (arrow) is most likely the anchor domain of HAP2 attached to domain D1 of flagellin. (**E**) Contoured map of the central section of the cylindrically averaged density. Going up along the filament axis, the continuous density of the inner tube (D0) stops (arrowhead) well before the continuous density of the outer tube (D1) reaches the plate of the cap. At this point, the outer tube wall becomes apparently thicker toward the inside (the thicker portion is indicated by vertical bar with terminal tics). This extra density can be attributed to the extension of the anchor domain of HAP2 into the cavity below the thin plate. Scale bar in (D), 100 Å.

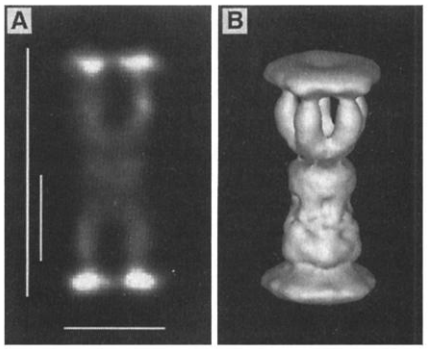

Fig. 3. Projection and three-dimensional density map of the HAP2 decamer formed in solution. (**A**) Averaged (composite) image of negatively stained particles, showing the bipolar arrangement of the two pentamers and the domain structure in each pentamer. Scale bars: left long, 290 Å; left short, 100 Å; bottom, 120 Å. (**B**) Solid surface representation of the three-dimensional density map. Two pentamer caps (top and bottom, each composed of a plate and five leg domains) are connected with a connector domain at the center, which is composed of both terminal regions that are disordered in the pentameric or monomeric form of HAP2 in solution. Only the upper pentamer was aligned and used for image reconstruction, because the connector domain has a significant azimuthal flexibility, and therefore, two pentamers are not well registered to each other. That is why the lower pentamer shows only a blurred image.

monomeric form of HAP2, are cleaved off, the fragment does not form the decamer (*30*). Only one-half of the decamer showed clear structural features; the other half showed a blurred image (Fig. 3B) because the connecting domain is relatively flexible, and we aligned only a portion containing a pentamer for the analysis. The flexible nature of the termini may be reflected in this connector flexibility.

In the cap-filament complex, the leg domains of the cap must be plugging into the cavity of the filament end to anchor the cap, as was suggested (*23*). Although individual leg domains were not discernible in the density map because of the limited resolution (Fig. 2), it appeared that four of the five indentations formed by domains D1 of flagellin were filled with the HAP2 leg domains, whereas the one with double indentation was not filled by the last leg domain (Fig. 4B). This leaves the inverted L-shaped opening fully open for flagellin assembly (Fig. 4B-1). This opening has the right size and shape and probably has an appropriate atomic surface structure for the newly arriving flagellin subunit to insert and bind, although it is probably large enough for HAP proteins to pass through. From the length of the axial domain of the HAP2 pentamer, which was longer than 100 Å (Fig. 3), the terminal regions of HAP2 are likely to extend further, deep into the cavity of the filament end, probably interacting with domains D0 of flagellin. This interaction seems to be important in stabilizing the cap-filament interaction, because the capping ability is completely lost upon truncation of the disordered terminal regions of HAP2 (*30*).

Because of the symmetry mismatch between the helical subunit array of the filament with 11 protofilaments forming the tube and the pentameric annular structure of the cap, the five leg domains of the cap must have significantly different conformations from one another for interaction with flagellin (*30*). This is indicated by the different ways in which the HAP2 leg domains fill the indentations at the end of the filament (Figs. 2C and 4B). The highly flexible nature of the leg domain, as partly indicated by the disordered terminal regions in the isolated cap (*30*), allows such polymorphic interactions, reducing conformational strains and permitting stable interactions between the two structures in spite of the symmetry mismatch. A few flagellin subunits at the very top show significant deviations in their positions from those of the ideal helical lattice, suggesting that a conformational flexibility of flagellin subunits may also contribute to further reducing the strains. At the same time, the high conformational entropy of the cap anchor domains would counterbalance the strong binding of the cap to the filament as a whole for efficient insertion of flagellin, as we discussed previously (*30*).

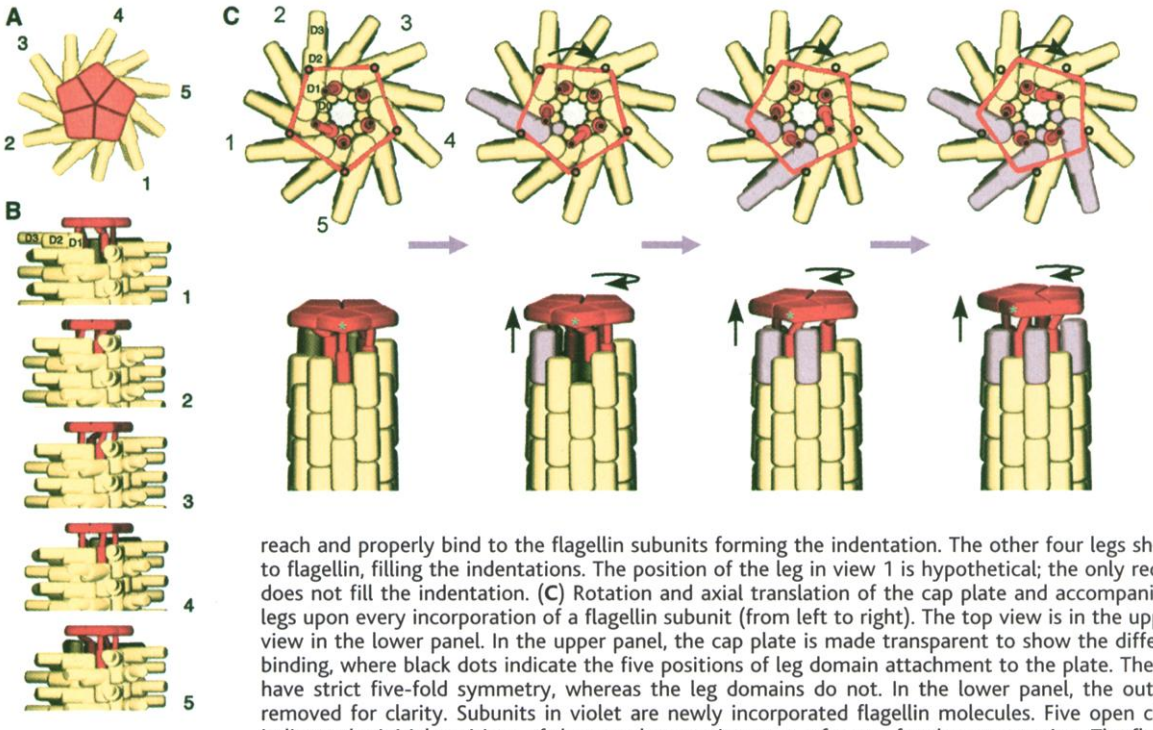

Fig. 4. Schematic diagram depicting the cap-filament binding and the rotary cap mechanism promoting the flagellin assembly. (**A**) Top view of the cap-filament complex. Numbers here as well as in (C) indicate the directions of views from the side in (B). (**B**) Five side views of the cap-filament complex, which correspond to the five views shown in Fig. 2C. The leg domain shown in view 1 cannot fill the inverted L-shaped indentation, because the indentation is too deep, and the leg cannot reach and properly bind to the flagellin subunits forming the indentation. The other four legs shown in views 2 to 5 bind to flagellin, filling the indentations. The position of the leg in view 1 is hypothetical; the only requirement is that this leg does not fill the indentation. (**C**) Rotation and axial translation of the cap plate and accompanied rearrangement of the legs upon every incorporation of a flagellin subunit (from left to right). The top view is in the upper panel, and an oblique view in the lower panel. In the upper panel, the cap plate is made transparent to show the different ways of leg domain binding, where black dots indicate the five positions of leg domain attachment to the plate. The plate and the black dots have strict five-fold symmetry, whereas the leg domains do not. In the lower panel, the outer domain of flagellin is removed for clarity. Subunits in violet are newly incorporated flagellin molecules. Five open circles in the upper panel indicate the initial positions of the cap plate vertices as a reference for the cap rotation. The flagellin assembly proceeds along the 1-start helix, which is in the counterclockwise direction when viewed from the top, approximately at every 65.5° (360*2/11). This is also the angle of rotation after which the next binding site appears. However, because the legs of the cap are located every 72° (360/5), a 6.5° clockwise rotation with permutation of the leg conformations is sufficient to make the appropriate interactions between the leg and flagellin subunits.

Every insertion of a flagellin subunit is likely to force the cap to move into the next stable position energetically equivalent to the current position. An obvious prediction from the present structure and our previous discussion (*30*) is that the cap moves up 4.7 Å and rotates 6.5° along the left-handed 5-start helix of the filament (Fig. 4C). In terms of the cap conformation, the next position is approximately 65.5° away along the right-handed 1-start helix. However, with permutation of the conformational states of the legs, which are 72° apart, a rotation of only 6.5° would suffice. This would result in a roughly complete rotation of the cap by the assembly of 55 flagellin subunits. At every subunit incorporation, four legs of the cap rearrange their conformations, and the last one changes its binding partner; that is, these legs walk along the helical steps of the filament end. These dynamic movements of the cap and its leg domains are required for efficient promotion of the flagellin self-assembly (*31*).

The energy for the cap rotation with the conformational rearrangements is presumably supplied by the binding energy of newly incorporated flagellin subunit to domains of flagellin and HAP2, where the binding occurs by concentration of flagellin within the channel by the type III export apparatus and the cap. The energy required for these movements would be relatively small, because the process would involve a number of small conformational rearrangements in sequence, where the energy would propagate from one to the next.

References and Notes

1. K. Namba, G. Stubbs, *Science* **231**, 1401 (1986).
2. D. L. D. Caspar, K. Namba, *Adv. Biophys.* **26**, 157 (1990).
3. F. Vonderviszt, S. Kanto, S.-I. Aizawa, K. Namba, *J. Mol. Biol.* **209**, 127 (1989).
4. K. Namba, F. Vonderviszt, *Q. Rev. Biophys.* **30**, 1 (1997).
5. H. C. Berg, R. A. Anderson, *Nature* **245**, 380 (1973).
6. M. Silverman, M. Simon, *Nature* **249**, 73 (1974).
7. S. H. Larsen *et al. Nature* **249**, 74 (1974).
8. T. Suzuki, T. Iino, T. Horiguchi, S. Yamaguchi, *J. Bacteriol.* **33**, 904 (1978).
9. T. Kubori *et al.*, *Science* **280**, 602 (1998).
10. F. Fan, K. Ohnishi, N. R. Francis, R. M. Macnab, *Mol. Microbiol.* **26**, 1035 (1997).
11. T. Minamino, R. M. Macnab, *J. Bacteriol.* **181**, 1388 (1999).
12. T. Iino, *J. Gen. Microbiol.* **56**, 227 (1969).
13. S. U. Emerson, K. Tokuyasu, M. I. Simon, *Science* **169**, 190 (1970).
14. M. Homma, T. Iino, *J. Bacteriol.* **162**, 183 (1985).
15. T. Ikeda *et al.*, *J. Bacteriol.* **169**, 1168 (1987).
16. M. Homma, H. Fujita, S. Yamaguchi, T. Iino, *J. Bacteriol.* **159**, 1056 (1984).
17. T. Ikeda, S. Asakura, R. Kamiya, *J. Mol. Biol.* **184**, 735 (1985).
18. M. Homma, T. Iino, *J. Bacteriol.* **164**, 1370 (1985).
19. The reconstituted cap-filament complex was prepared as previously described (*23*). We collected about 600 images of frozen hydrated cap-filament complex with a JEOL JEM-3000SFF electron microscope with its field emission gun operated at 300 kV and the specimen temperature of 4 to 40 K. Images were recorded on SO-163 film (Eastman Kodak Co., Rochester, NY) at a magnification of ×50,000. The electron dose was ~25 e/Å^2. The collection of many good images of the cap-filament complex was extremely time-consuming, because the number density in each film was limited by the long filaments to which the caps are attached. Reconstituted cap-filament specimen with relatively short filament was therefore used to increase the number density on grids. Images were digitized with LeafScan 45 (Leaf Systems, Southboro, MA) at a step size of 10 μm and reduced by a factor of 2. Most of the image analysis was carried out by using the SPIDER/WEB package (*32*), a modified version of MRC helical package (*33*), and the Brandeis helical package (*34*). By standard two-dimensional alignment procedure, however, the cap position and filament axis were misaligned, because the projection pattern of the helical lattice of the filament, which dominates the two-dimensional cross-correlation, is variable, depending on the azimuthal orientation of the filament. Therefore, we devised a new alignment method that uses one-dimensional projection for alignment in each axis perpendicular to the projection axis. For in-plane rotation alignment, a running average along the approximate filament axis was used to smear out the helical lattice feature. The azimuthal orientation, which was needed for the three-dimensional reconstruction, was determined by using the helical lattice of the filament (*35*). Of 589 images used for two-dimensional alignment and an average composite, the result of which is shown in Fig. 1C, 425 images were used to produce a three-dimensional density map by back projection. The remaining 164 images were rejected, because the difference in the phase residuals obtained by fitting the filament portion of the image to a reference image oriented in the two opposite polarities was smaller than a certain preset value, and therefore, the image quality was judged insufficient. The resolution was determined to be 27 Å by the Fourier shell correlation method, with a cut-off of 0.5. More detailed description of the data collection and analysis will be given elsewhere.
20. Y. Mimori *et al.*, *J. Mol. Biol.* **249**, 69 (1995).
21. D. G. Morgan, C. Owen, L. A. Melanson, D. J. DeRosier, *J. Mol. Biol.* **249**, 88 (1995).
22. K. Imada *et al.*, *J. Mol. Biol.* **277**, 883 (1998).
23. S. Maki *et al.*, *J. Mol. Biol.* **277**, 771 (1998).

24. I. Yamashita *et al.*, *J. Mol. Biol.* **253**, 547 (1995).
25. Y. Mimori-Kiyosue, F. Vonderviszt, K. Namba, *J. Mol. Biol.* **270**, 222 (1997).
26. I. Yamashita *et al.*, *Nature Struct. Biol.* **5**, 125 (1998).
27. Z. Xu, A. L. Horwich, P. B. Sigler, *Nature* **388**, 741 (1997).
28. T. Ikeda, K. Oosawa, H. Hotani, *J. Mol. Biol.* **259**, 679 (1996).
29. The decameric complex of HAP2 was prepared as previously described (*23*). We collected about 400 images of negatively stained specimen with a JEOL JEM-1010 electron microscope at 100 kV and a magnification of ×75,000. Image analysis was carried out as briefly described in the following section. After two-dimensional alignment of 319 images, azimuthal orientation of the decamer was initially determined by using the plate portion of the cap-filament structure as the reference, and the three-dimensional image was reconstructed by back projection with five-fold symmetry enforced. The orientation was further refined by using the pentameric half of this structure as the reference, and the three-dimensional image was reconstructed again. This process was repeated four times, and the final three-dimensional image was reconstructed from 304 images. More detailed description of the analysis will be given elsewhere.
30. F. Vonderviszt *et al.*, *J. Mol. Biol.* **284**, 1399 (1998).
31. Animation of the cap rotation promoting in vivo flagellin self-assembly can be seen at www.npn.jst.go.jp/yone.html and by *Science* Online subscribers at www.sciencemag.org/cgi/content/full/290/5499/2148/DC1.
32. J. Flank *et al.*, *J. Struct. Biol.* **116**, 190 (1996).
33. C. Toyoshima, N. Unwin, *J. Cell Biol.* **111**, 2623 (1990).
34. C. H. Owen, D. G. Morgan, D. J. DeRosier, *J. Struct. Biol.* **116**, 167 (1996).
35. D. Thomas, thesis, Brandeis University (1999).
36. We thank K. Murata and Y. Fujiyoshi for technical advice in electron cryomicroscopy; T. R. Shaikh and D. Thomas for helpful comments in image analysis; and T. Nitta and F. Oosawa for continuous support and encouragement. F.V. was partly supported by the Hungarian OTKA T025468 grant.

16 August 2000; 2 November 2000

Development of CD8α-Positive Dendritic Cells from a Common Myeloid Progenitor

David Traver,[1]* Koichi Akashi,[2]* Markus Manz,[1]*† Miriam Merad,[1] Toshihiro Miyamoto,[1] Edgar G. Engleman,[1] Irving L. Weissman[1]

Dendritic cells (DCs) are critical in both initiating adaptive immune responses and maintaining tolerance to self antigens. These apparently contradictory roles have been suggested to depend on different subsets of DCs that arise from either myeloid or lymphoid hematopoietic origins, respectively. Although DC expression of CD8α is attributed to a lymphoid origin, here we show that both CD8α$^+$ and CD8α$^-$ DCs can arise from clonogenic common myeloid progenitors in both thymus and spleen. Thus, expression of CD8α is not indicative of a lymphoid origin, and phenotypic and functional differences among DC subsets are likely to reflect maturation status rather than ontogeny.

Dendritic cells (DCs) are specialized antigen-presenting cells that both orchestrate specific immune responses (*1*, *2*) and delete potentially autoreactive T cells (*3*, *4*). These seemingly contradictory functions have been suggested to result from the actions of different DC subsets (*5*, *6*). Recently, murine DCs have been subdivided into at least two populations, myeloid and lymphoid, on the basis of anatomic localization (*7*, *8*), transplantation experiments (*3*), and cell surface phenotypes (*8*, *9*). DCs bearing the CD11c$^+$ MHCII$^+$ Mac-1$^+$ CD8α$^-$ cell surface markers (hereafter referred to as CD8α$^-$ DCs) can efficiently derive from myeloid precursors (*10*). Alternatively, DCs bearing the CD11c$^+$ MHCII$^+$ Mac-1$^-$ CD8α$^+$ cell surface phenotype (hereafter referred to as CD8α$^+$ DCs) can arise at low frequencies from thymic T cell progenitors (*3*). It has been proposed that myeloid DCs direct adaptive immune responses whereas lymphoid DCs eliminate self-reactive lymphocytes, suggesting that DC ontogeny underlies these largely nonoverlapping functions (*5*).

Both clonogenic common lymphoid progenitors [CLPs, ~0.02% of whole bone marrow (BM)] (*11*) and clonogenic common myeloid progenitors (CMPs, ~0.2% of whole BM) (*12*) have been isolated and respectively give rise to each of the major branches of the hematopoietic system (*13*). The transplantation of 2×10^4 CMPs (contained within 1×10^7 BM cells) into CD45 congenic mice (Fig. 1A) showed abundant DC reconstitution of recipient spleens, lymph nodes (LNs), and thymi. Recipient spleens showed an average of 1×10^4 CD8α$^-$ DCs and 8×10^4 CD8α$^+$ DCs at 17 days after transplantation (Fig. 1, B and C), the numerical peak for CMP-derived DCs. Recipient thymi contained an average of 2×10^3 CMP-derived DCs, all of which were CD8α$^+$ (Fig. 2E).

CMP-derived CD8α$^+$ DCs expressed the costimulatory markers characteristic of active DCs, including CD40, CD80, CD86, and Dec205 (Fig. 2, A to D). CMP-derived

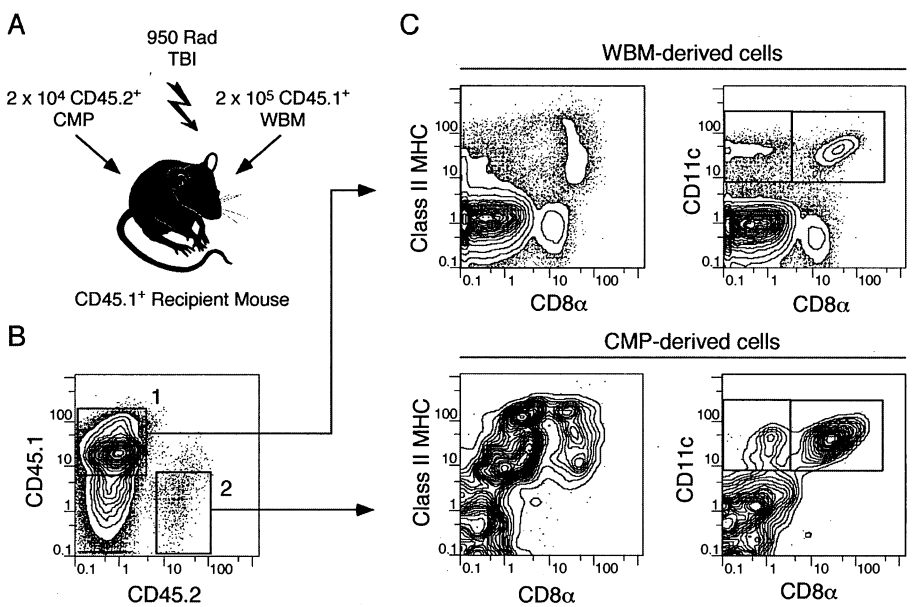

Fig. 1. Common myeloid progenitors (CMPs) give rise to CD8α$^+$ DCs. (**A**) CMPs were stained, sorted, and competitively transplanted into lethally irradiated CD45 congenic animals along with host-type whole bone marrow (WBM) as described (*12*). (**B**) CD45 expression was used to gate on host-type (CD45.1) or donor-type (CD45.2) splenocytes at 17 days after transplantation. (**C**) Analysis of DC phenotype arising from WBM (gate 1) or CMPs (gate 2).

[1]Department of Pathology and Department of Developmental Biology, Stanford University, Stanford, CA 94305, USA. [2]Department of Cancer Immunology and AIDS, Dana-Farber Cancer Institute, Boston, MA 02115, USA.

*These authors contributed equally to this work.
†To whom correspondence should be addressed. E-mail: manz@stanford.edu